Available free online at www.medjchem.com

Mediterranean Journal of Chemistry

Mediterranean Journal of Chemistry **2022**, 12(2), 123-139

Copper corrosion inhibition in nitric acid solution by 2-(1,3-dihydrobenzimidazol-2-ylidene) -3-oxo-3-(pyridin-3-yl) propanenitrile: Gravimetric, Quantum chemical and QSPR studies

Mougo André Tigori [1,*], Aboudramane Koné [1], Koua N'zebo René [1], Mamadou Yeo [2] and Paulin Marius Niamien [2]

[1] Laboratoire des Sciences et Technologies de l'Environnement, UFR Environnement, Université Jean Lorougnon Guédé, BP 150 Daloa, Côte d'Ivoire

[2] Laboratoire de Constitution et de Réaction de la Matière, UFR SSMT, Université Félix Houphouët-Boigny, 22 BP 582 Abidjan 22, Côte d'Ivoire

Abstract: The metal corrosion threat in the metallurgical industry is becoming increasingly important. So in this work, the inhibition properties of 2-(1,3-dihydrobenzimidazol-2-ylidene)-3-oxo-3-(pyridin-3-yl) propanenitrile for copper corrosion in 1 M nitric acid medium were evaluated by mass loss technique, density functional theory (DFT) and quantitative structure-property relationship (QSPR) model. The results show that this compound was excellent anticorrosive properties with a maximum inhibition efficiency of 89.39 % for a concentration of 0.2 mM at 323 K. The inhibition efficiency increases with increasing temperature and inhibitor concentration. Adsorption isotherms reported that the molecule adsorbs on copper surface according to Langmuir isotherm. Thermodynamic adsorption and activation parameters were determined and analyzed. They revealed spontaneous adsorption and a strong interaction between the molecule and copper surface. DFT calculations at the B3LYP level with 6-31G(d,p) and 6-311G(d,p) basis set permitted to explain the electronic exchanges between molecule and copper, thus justifying the experimentally obtained inhibition efficiency values. A local reactivity study of molecules indicated that N (29) and C (7) atoms are the likely sites for nucleophilic and electrophilic attacks, respectively. In addition, QSPR model was used to correlate experimental inhibition efficiency with the descriptor parameters of the studied molecule, and it is found that the calculated inhibition efficiencies are close to experimental inhibition efficiencies. Finally, this study showed a good correlation between theoretical and experimental data.

Keywords: 2-(1,3-Dihydrobenzimidazol-2-ylidene)-3-oxo-3-(pyridin-3-yl); Copper corrosion; Mass loss; Density functional theory; Quantitative structure-property relationship.

1. Introduction

Copper has a wide application in industries due to its remarkable physical, mechanical, anticorrosive, and biological properties [1,2]. For example, it is used in manufacturing electronic equipment, automotive equipment, building materials, plumbing and piping equipment, industrial equipment, and coin manufacture. In addition, the pleasing appearance of copper and its alloys lends a touch of quality, even prestige, to the design of public spaces, furniture, objects, and decorative items. However, acid washing is performed periodically to descale and clean these copper metal systems to maintain this quality touch. Unfortunately, industrial use of acid solutions in many mechanical processes causes copper dissolution [3,4]. This dissolution is greatly enhanced in the petroleum industry, where etching and acid stripping promote corrosion of the metals involved. Nitric acid is commonly used to perform these pickling operations, so the search for compounds to add to these solutions to control copper dissolution during these different operations in an industrial setting is important.

Within this framework, copper protection and maintenance are necessary. Among the various corrosion prevention methods, the inhibitors seem to be the most practical and convenient method to increase corrosion resistance [5,6]. However, some inhibitors are toxic. Therefore, the natural organic compounds used to preserve the environment, either synthesized or extracted from aromatic herbs and medicinal plants, are favored [7-10]. These compounds generally have π bonds and heteroatoms (P, S, N, and O) and can promote electronic exchanges

**Corresponding author: Mougo André Tigori*
Email address: tigori20@yahoo.fr
DOI: http://dx.doi.org/10.13171/mjc02209131649tigori

Received August 20, 2022
Accepted September 5, 2022
Published September 13, 2022

between the inhibitor and the metal [11,12]. These exchanges participate in the formation of a protective barrier on the metal surface.

Therefore, the present work investigated 2-(1,3-dihydrobenzimidazol-2-ylidene)-3-oxo-3-(pyridin-3yl) propanenitrile anticorrosive properties for copper corrosion in 1 M nitric acid solution. The choice of this compound in this study resides in the fact that it presents a large molecular surface with heteroatoms (N and O) and would be less toxic because it is an antifungal agent that belongs to the series of benzimidazolyl 2-cyanochalcones. Indeed, this molecule has been used to fight opportunistic mycotic infections due to development in humans or animals because of the strong resistance that triazole derivatives presented [13,14]. Currently, concerning environmental preservation and the search for non-toxic inhibitors, the drugs are ideal candidates to fight against metal corrosion. Several studies have proven the inhibition performance of some drugs [15-17]. This study will also aim to prove the inhibition behavior of this antifungal. This choice is also because this compound can be synthesized with cheap raw materials.

Metal-inhibitor interactions are associated with many complex processes that can be studied at the molecular level using appropriate models such as density functional theory (DFT). This theory, which is based on quantum chemicals, has become a means to elucidate the mechanism and a tool to predict organic molecules' behavior in corrosion process control [18-20]. Thus in recent years, Density Functional Theory (DFT) has become a reliable and inexpensive method used in corrosion inhibition. While the quantitative structure-property relationship (QSPR) predictive model [21] highlights the correlation between theoretical molecular parameters and experimental results.

2. Experimental

2.1. Material

2.1.1. Inhibitor molecule

The inhibitor molecule used in our work is 2-(1,3-dihydrobenzimidazol-2-ylidene)-3-oxo-3-(pyridin-3-yl) propanenitrile (formula $C_{15}H_{10}ON_4$). Its structure is given in Figure 1. This molecule is of the benzimidazolyl 2-cyanochalcone series. The molecular weight is M = 262.27 g/mol. This organic compound has been synthesized in the Laboratory according to a series of methods [22,23]. Its molecular structure was identified by: RMN-^{1}H, ^{13}C, spectroscopies, and mass spectroscopy.

RMN ^{1}H (DMSO-d6, δ ppm): 8.40 (1H, s, C=CH).
^{13}C: 145.14 (C=CH); 116.04 (C≡N); 102.38 (C=CH).
SM [EI, 70 eV]: 245 ($[M]^+$, 39); 244 ($[M-H]^+$, 96).
Washing in hexane: 52 %. mp: 222°C.

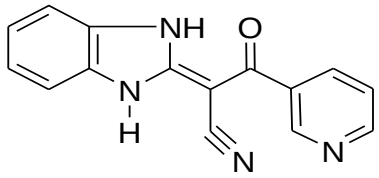

Figure 1. Chemical structure of 2-(1,3-dihydrobenzimidazol-2-ylidene)-3-oxo-3-(pyridin-3-yl) propanenitrile (DBP)

2.1.2. Chemical solutions

Analytical grade 70 % nitric acid from FISHER was used to prepare the corrosive solution. The solution was prepared by diluting the commercial nitric acid solution using distilled water. The blank was a 1M HNO_3 solution. From this corrosive solution, we prepared four concentrations of the compound 2-(1,3-dihydrobenzimidazol-2-ylidene)-3-oxo-3-(pyridin-3-yl) propanenitrile, which are 0.04 mM, 0.06 mM, 0.14 mM and 0.2 mM.

2.1.3. Copper samples preparation

Copper samples used in this study were in the form of a rod measuring 10 mm in length and 2.2 mm in diameter with mass m = (0.2338 ± 0.0001) g; they were cut from commercial copper of 99.5 % purity. The copper samples were polished with silicon carbide abrasive paper ranging in size from 150 to 600, rinsed with distilled water, cleaned with acetone, and rinsed with distilled water before being dried in an oven (MEMMERT) at 80°C. Then, pre-treated samples were kept in a desiccator without humidity and weighed with Analytical Balance (KERN) of accuracy ± 0.1mg.

2.2. Mass loss method

For gravimetric tests, pre-treated samples were immersed in 50 mL 1 M HNO_3 with or without the tested compound. A Selecta water thermostat (RAYPA) ± 0.5°C is controlled to maintain temperatures ranging from 25°C to 50°C. After 1 hour, the samples were removed, washed with distilled water, dried, stored in a desiccator, and reweighed. All tests were performed in aerated solutions. From the mass loss values, the average copper corrosion rate (W), material recovery rate (θ), and inhibitor inhibition efficiency (IE (%)). These different quantities will be determined according to the inhibitor concentration and medium reaction

temperature. The following expressions are used to determine these quantities:

$$W = \frac{\Delta m}{S_e.t} = \frac{m_1 - m_2}{S_e.t} \quad (1)$$

$$\theta = \frac{W_0 - W}{W_n} \quad (2)$$

$$IE(\%) = \frac{W_0 - W}{W_n} * 100 \quad (3)$$

Δm: mass loss (g), m_1, and m_2 are, respectively, the masse (g) before and after immersion in solution test; t: immersion time (h); Se: the total surface of the sample (cm^2); w_0 and w; are respectively the copper corrosion rates in absence and presence of 2-(1,3-dihydrobenzimidazol-2-ylidene)-3-oxo-3-(pyridin-3-yl) propanenitrile.

2.3. Quantum chemistry calculations

Quantum chemistry calculations were performed with Gaussian 09 software [24] in 6-31G (d,p) and 6-311G (d, p) bases and using the hybrid functional B3LYP, a version of density functional theory (DFT) that uses the three-parameter Becke functional (B3) with a mixture of Hartree-Fock and DFT exchange terms associated with the gradient-corrected correlation function of Lee et *al.* [25,26]. Indeed, DFT considers the electronic correlation, and the results are better than those obtained with the Hartree-Fock method for similar computation times. Furthermore, the complete optimization of molecule geometry has been performed at B3LYP/6-31G (d,p) level.

The calculations were performed in the gas phase and allowed to determine: Quantum chemical descriptors, including LUMO energy (E_{LUMO}), HOMO energy (E_{HOMO}), energy gap (ΔE), dipole moment (μ), and Mulliken atomic charges. Furthermore, the reactivity parameters such as ionization energy (I), electronic affinity (A), electronegativity (χ), global hardness (η), global softness (σ), and the fraction of electrons transferred (ΔN) were derived from the quantum chemical descriptors. Fukui indices were determined from Mulliken atomic charges.

Indeed, density functional theory (DFT) states that electronic properties can be described in terms of electron density functionals by locally applying appropriate relations to a homogeneous electronic system. This theory states that changes in electronic energy $dE[\rho(r)]$ are related to changes in the number of electrons N and changes in external potential $v(r)$ felt by the electron distribution density functional theory (DFT), expressed as follows:

$$dE[\rho(r)] = \mu_p dN + \int \rho(r) dv(r) dr \quad (4)$$

The chemical potential, which is opposite to electronegativity (χ), is equal to the first derivative of energy concerning electrons number and defined by the following relation [27]:

$$\mu_P = \left(\frac{\partial E}{\partial N}\right)_{v(r)} = -\chi \quad (5)$$

Using Koopmans's theorem [28], ionization potential (I) and electron affinity (A) of DBP are calculated using the following expressions:

$$I = -E_{HOMO} \quad (6)$$

$$A = -E_{LUMO} \quad (7)$$

The energy gap (ΔE) between the two energies (LUMO-HOMO) can be used as a measure of molecule excitability. It is defined by:

$$\Delta E = E_{LUMO} - E_{HOMO} \quad (8)$$

Electronegativity [29], which measures the power of an atom or a group of atoms to attract electrons towards itself, can be written as:

$$\chi = \frac{I+A}{2} = -\frac{E_{LUMO}+E_{HOMO}}{2} \quad (9)$$

Global hardness (η) measures the resistance of an atom to charge transfer [29] can be assessed by the following equation:

$$\eta = \frac{I-A}{2} = \frac{E_{LUMO}-E_{HOMO}}{2} \quad (10)$$

Global softness (σ) is the inverse of global hardness (η); itt measures the ability of an atom or a group of atoms to receive electrons [29]. It is formulated as follows:

$$\sigma = \frac{1}{\eta} = \frac{2}{I-A} \quad (11)$$

The fraction of electrons transferred between the inhibitor molecule and the metal (ΔN) is calculated according to the Pearson electronegativity relation [30]:

$$\Delta N = \frac{\chi_{cu} - \chi_{inh}}{2(\eta_{cu} + \eta_{inh})} \quad (12)$$

In this case χ_{cu} and χ_{inh} denote the absolute electronegativity of copper and inhibitor molecule, respectively. The calculations were performed using the following theoretical values: χ_{cu} = 4.98 eV [31] and η = 0 [32].

The electrophilicity index (ω), which characterizes the ability of a compound to accept or donate [33] electrons, can be calculated by:

$$\omega = \frac{\mu_P^2}{2\eta} = \frac{(I+A)^2}{4(I-A)} \quad (13)$$

Jose´L. Gazquez et al. [34] introduced new descriptors derived from electron affinity (A) and ionization potential (I) to explain the electron donating and accepting character of a chemical species.

Thus the ability of a molecule to accept electrons or charge is related by electroaccepting power (ω^+), which is expressed as follows:

$$\omega^+ = \frac{(I+3A)^2}{16(I-A)} \quad (14)$$

As for the character of a molecule to give electrons or charge defined by electrodonating power ω^- and is expressed by:

$$\omega^- = \frac{(3I+A)^2}{16(I-A)} \quad (15)$$

Local reactivity descriptors derived from DFT have been widely used to predict the most reactive molecular sites for the electrophilic, nucleophilic, or concerted attack. These local descriptors are based on Fukui functions and dual descriptors.

Fukui function is defined as the derivative of the electron density (r) concerning N, the total number of electrons in the system, at constant external potential V(r) acting on an electron due to all the nuclei in the system [35]:

$$f(r) = \left(\frac{\partial \rho(r)}{\partial N}\right)_{v(r)} = \left(\frac{\delta \mu_P}{\partial v(r)}\right)_N \quad (16)$$

Fukui functions $f^+(r)$ and $f^-(r)$ are calculated according to the following finite difference approximation [35] equal to the electron densities of LUMO and HOMO orbitals, respectively:

Nucleophilic attack

$$f_k^+ = q_k(N+1) - q_k(N) \quad (17)$$

Electrophilic attack

$$f_k^- = q_k(N) - q_k(N-1) \quad (18)$$

Where $q_k(N+1)$ $q_k(N-1)$ is the electronic population of atoms k in cationic, neutral, and anionic forms, respectively.

Dual descriptor unambiguously identifies the likely sites for nucleophilic and electrophilic attacks [36,37]. It can be calculated using the following equation.

$$\Delta f_k(\mathrm{r}) = \left(\frac{\partial f_k(r)}{\partial \mathrm{N}}\right)_{\mathrm{v(r)}} \quad (19)$$

The equation gives the condensed form of the dual descriptor:

$$\Delta f_k(\mathrm{r}) = f_k^+ - f_k^- \quad (20)$$

2.4. Quantitative Structure-Property Relationship (QSPR) details

To study DPB experimental behavior and to predict the behavior of analogous molecules to the studied compound, quantitative structure-property relationship (QSPR) has been used in this work. In fact, QSPR model is a mathematical approach that attempts [38] to correlate experimental inhibition efficiencies of DPB with its quantum chemical parameters determined from DFT. We used the non-linear model of Lukovits et *al.* [39,] which is given as follows:

$$IE_{calc}(\%) = \frac{[Ax_j+B]C_i}{1+[Ax_j+B]C_i} * 100 \quad (21)$$

In this case, C_i represents different concentrations for inhibitor, which are 40 μM, 60 μM, 140 μM, and 200 μM, A and B are real constants that will be determined when solving the system of equations. We tested sets of three parameters (x_1, x_2, x_3). Then the equation becomes:

$$IE_{calc}(\%) = \frac{[Ax_1+Bx_2+Dx_3+E]C_i}{1+[Ax_1+Bx_2+Dx_3+E]C_i} * 100 \quad (22)$$

This equation permits a system of four equations with four unknowns A, B, D, and E. It is thus a question of finding for the molecule the set of coefficients A, B, D, and E, which permits obtaining the value of the inhibition efficiency closest to the experimental value. The calculations were carried out using the EXCEL software.

3. Results and Discussion

3.1. Gravimetric studies

3.1.1. Corrosion rates and inhibition efficiency

Figures 2 and 3 show copper corrosion rate and inhibition efficiency evolution versus concentration for DBP at different temperatures.

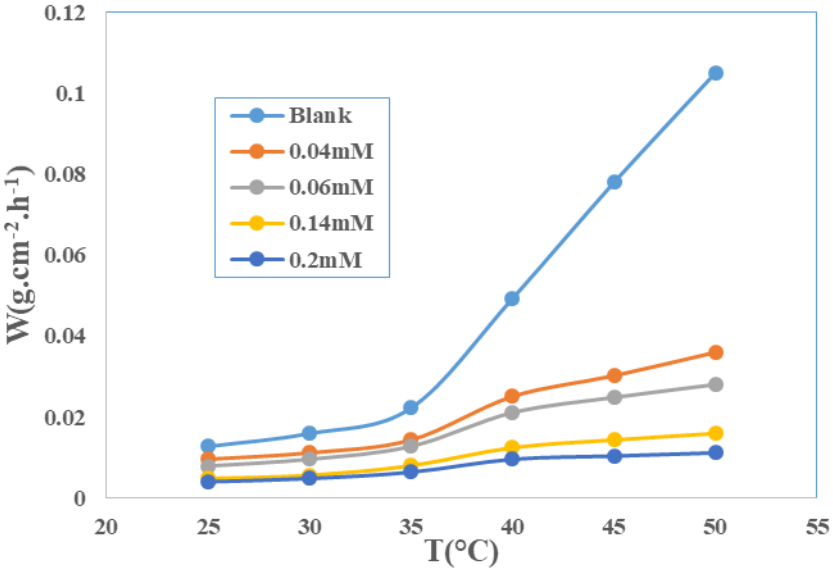

Figure 2. Copper corrosion rate versus concentration for different temperatures

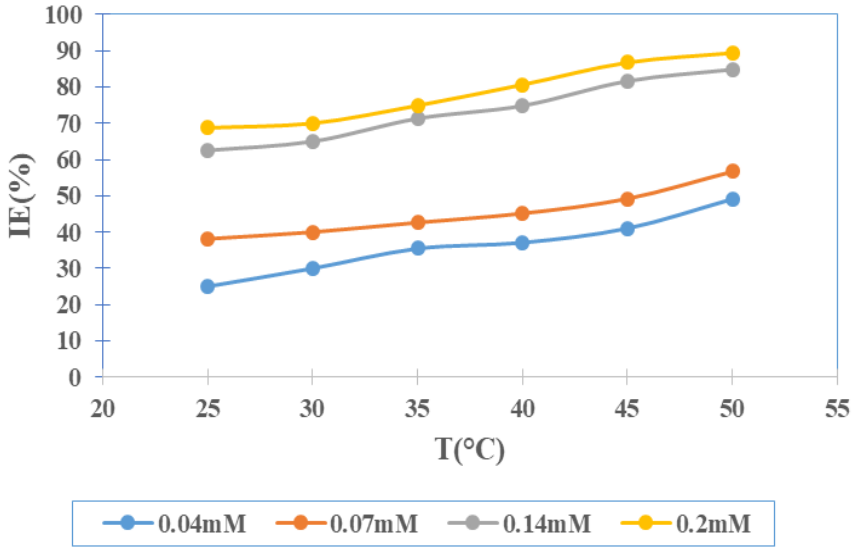

Figure 3. The inhibition efficiency of DBP versus temperature for different concentrations

Figure 2 shows that the copper corrosion rate regularly decreases as the inhibitor concentration increases and increases with increasing temperature. However, this rate is very high in DBP absence. This means that the copper corrosion is sufficiently reduced when the concentration DBP increases.

Figure 3 shows that the inhibition efficiency increases with DBP concentration and temperature.

When the inhibitor concentration increases, the coverage rate of the copper surface increases. This coverage rate may be due to molecule adsorption of the metal surface. Similar results have been obtained in the literature [40].

The copper surface is thus covered with a protective film layer, isolating it from the aggressive environment.

These results highlight the excellent DBP inhibitory power in 1 M HNO_3 solution copper corrosion control. Furthermore, the highest inhibition efficiency obtained for 0.2 mM and T = 323 K is 89.39 %, confirming that DBP is effective at high temperatures.

3.1.2. Adsorption isotherms and thermodynamic parameters details

We used adsorption isotherms to study the relationship between the amount of DBP adsorbed on the copper surface and its concentration in phase in contact with metal at a constant temperature. Thus, several isotherms were tried, namely Langmuir, El-Awady, Temkin and Freundlich isotherms. These tests to fit the experimental data showed Langmuir isotherm is the best. Indeed the determination coefficients (R^2) of the lines obtained in the Langmuir isotherm case are closer to unity

than those of other isotherms studied (El-Awady, Temkin, and Freundlich). The equation of this isotherm is given by the following relation [41]:

$$\frac{C_{inh}}{\theta} = \frac{1}{K_{ads}} + C_{inh} \quad (23)$$

Where: inhibitor concentration and adsorption equilibrium constant.

Figure 4 gives the representation of the plot of Langmuir adsorption isotherm.
The regression parameters of straight lines obtained are recorded in Table 1.

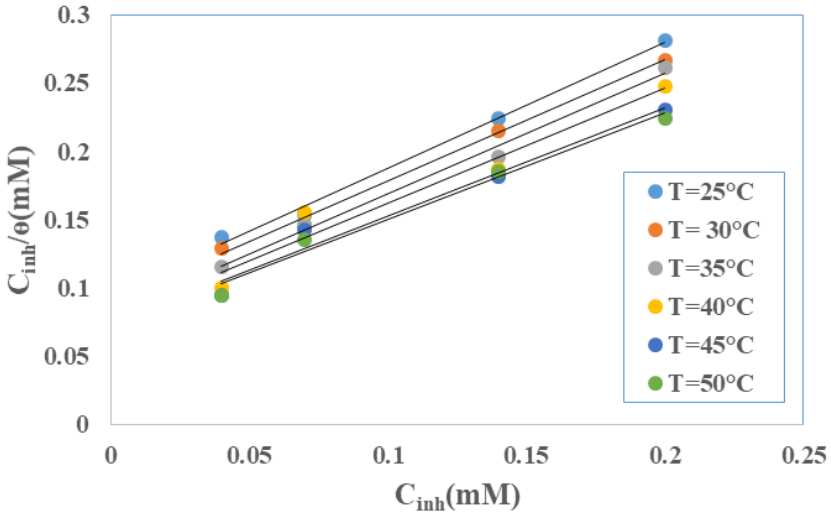

Figure 4. Langmuir's adsorption isotherm plots of DBP on copper in 1 M HNO_3

Table 1. Langmuir adsorption isotherm parameters.

Temperature (K)	Equation	R^2
298	$\frac{C_{inh}}{\theta} = 0.9227C_{inh} + 0.0951$	0.9952
303	$\frac{C_{inh}}{\theta} = 0.8887C_{inh} + 0.0892$	0.9949
308	$\frac{C_{inh}}{\theta} = 0.8869C_{inh} + 0.0800$	0.9921
313	$\frac{C_{inh}}{\theta} = 0.841C_{inh} + 0.0779$	0.9526
318	$\frac{C_{inh}}{\theta} = 0{,}7905C_{inh} + 0.0734$	0.9707
323	$\frac{C_{inh}}{\theta} = 0.7787C_{inh} + 0.072$	0.9818

By analyzing Table 1, we observed that the straight lines slopes of this isotherm were almost equal to unity. So DBP adsorbs on copper according to Langmuir isotherm. In this case, the adsorption is monolayer, and the interactions between adsorbed particles are negligible.

Using the equations in Table 1, we determined the adsorption constants (K_{ads}). The changes in standard adsorption-free enthalpy (ΔG^0_{ads}) were calculated using the following equation [42]:

$$\Delta G^0_{ads} = -RTln(55.5\ K_{ads}) \quad (24)$$

Where R is the gas constant, T is the absolute temperature, and 55.5 is the concentration of water (in mol/L) in the solution.

Standard enthalpy change (ΔH^0_{ads}) and the standard entropy change (ΔS^0_{ads}) were determined by plotting of ΔG^0_{ads} versus temperature (figure 5) from the equation:

$$\Delta G^0_{ads} = \Delta H^0_{ads} - T\Delta S^0_{ads} \quad (25)$$

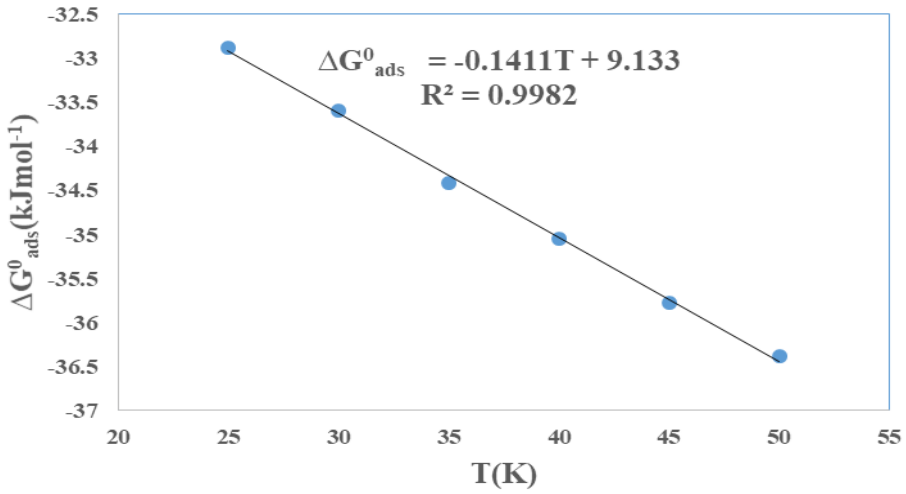

Figure 5. ΔG^0_{ads} versus temperature for DBP adsorption on copper in 1 M HNO_3

The different values of adsorption constants and Thermodynamic Adsorption parameters are recorded in Table 2.

Table 2. Thermodynamic Adsorption parameters.

T(K)	$K_{ads}(M^{-1})$	$\Delta G^0_{ads}(kJ\ mol^{-1})$	$\Delta H^0_{ads}(kJ\ mol^{-1})$	$\Delta S^0_{ads}(J\ mol^{-1}K^{-1})$
298	10515.2471	-32.8788	9.1330	141.1000
303	11210.7623	-33.5917		
308	12468.8279	-34.4183		
313	12836.9704	-35.0527		
318	13623.9782	-35.7699		
323	13888.8888	-36.3900		

The standard free energy change of adsorption (ΔG^0_{ads}) values are negative, which can characterize the interaction of adsorbed molecules with the metal surface, showing that the adsorption of the inhibitor on copper is spontaneous and the stability of adsorbed layer [43]. These values decrease with increasing temperature, indicating an increase in intensities at the interactions between adsorbed molecules with temperature. This increase could justify the high values of inhibition efficiencies obtained experimentally. An increase in the equilibrium constant (K_{ads}) is also observed with increasing temperature, indicating that the rise in temperature favors DBP adsorption on the copper surface. Moreover, free energy change of adsorption values ranges from -32.87 $kJ.mol^{-1}$ to -36.38 $kJ.mol^{-1}$, thus showing the two adsorption modes for the molecule; [43] physisorption and chemisorption. The standard enthalpy change (ΔH^0_{ads}) is positive, reflecting the endothermic character of DBP adsorption on copper surface [44]. The values ΔS^0_{ads} are positive; this reveals that the disorder increases during DBP adsorption on copper [44]. This disorder is related to the water molecules' desorption which is replaced by inhibitor molecules.

3.1.3. Adejo–Ekwenchi isotherm

To determine the adsorption nature and the temperature domains affiliated with this nature, Adejo-Ekwenchi isotherm [45] was used. The characteristic equation of this model is as follows:

$$log\left(\frac{1}{1-\theta}\right) = logK_{AE} + blogC_{inh} \quad (26)$$

Where K_{AE} and b are Adejo-Ekwenchi isotherm parameters.

The curves of this model are obtained by plotting $log\left(\frac{1}{1-\theta}\right)$ versus $logC_{inh}$.

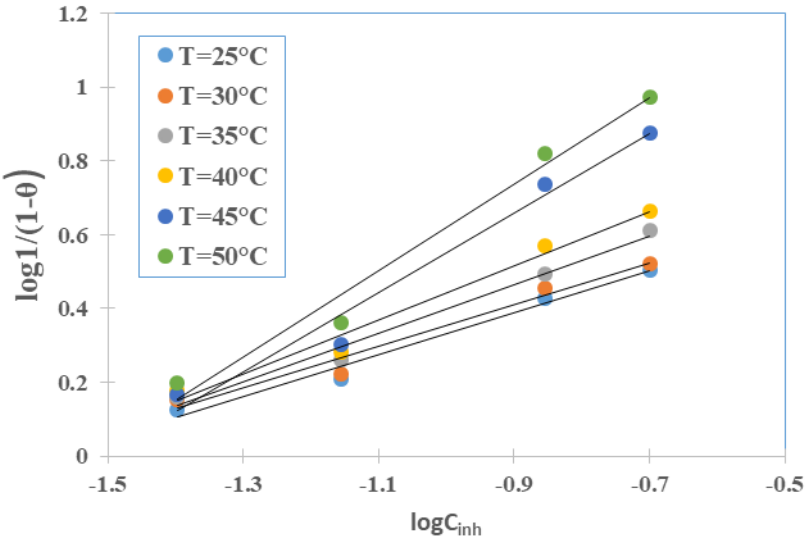

Figure 6. $log\left(\frac{1}{1-\theta}\right)$ versus $logC_{inh}$

The regression parameters of the obtained lines are recorded in Table 3.

Table 3. Parameters of Adejo-Ekwenchi isotherm plots.

T (K)	R^2	b	$logK_{AE}$	K_{AE}
298	0.9818	0.5685	0.8997	7.9377
303	0.9682	0.5689	0.9157	8.2356
308	0.9845	0.6577	1.0560	11.3762
313	0.9781	0.7315	1.1738	14.9210
318	0.9730	1.0722	1.6220	41.8793
323	0.9787	1.1648	1.7850	60.9536

Table 3 examination shows that determination coefficients (R^2) are close to unity. These values confirm the applicability of this model. Furthermore, parameter b values are increasing, disclosing that the adsorption process is dominated by chemisorption [45].

3.1.4. Effect of temperature and activation parameters

The temperature has a great influence on the corrosion rate of a metal. The activation parameters that depend on the temperature permit understanding the inhibitor adsorption activity. So, the temperature dependence of the corrosion rate can be expressed by the Arrhenius equation:

$$W = A.exp\left(-\frac{E_a}{R.T}\right) \quad (27)$$

This equation can also be expressed according to the following relation:

$$logW = logA - \frac{E_a}{2.3.R.T} \quad (28)$$

Where W is the corrosion rate, E_a is the activation energy, R is the universal gas constant, T is the absolute temperature, and A is the frequency factor.

Activation enthalpy(ΔH_a^*) and activation entropy ΔS_a^* of the corrosion process is also calculated using the Eyring transition state equation in the following form:

$$W = \frac{R.T}{\aleph.h} exp\left(\frac{\Delta S_a^*}{R}\right).exp\left(-\frac{\Delta H_a^*}{R.T}\right) \quad (29)$$

The logarithmic form of this expression leads to:

$$log\left(\frac{W}{T}\right) = log\left(\frac{R}{\aleph.h}\right) + \frac{\Delta S_a^*}{2.3.R} - \frac{\Delta H_a^*}{2,3.R.T} \quad (30)$$

Where ΔS_a^* is the activation entropy, ΔH_a^* is the activation enthalpy, R is the perfect gas constant, $\aleph$ is Avogadro number, and h is Planck's constant.

The representation of log (W) versus (1/T) and the transition state plots of log (W/T) versus (1/T) are given respectively in Figures 7 and 8.

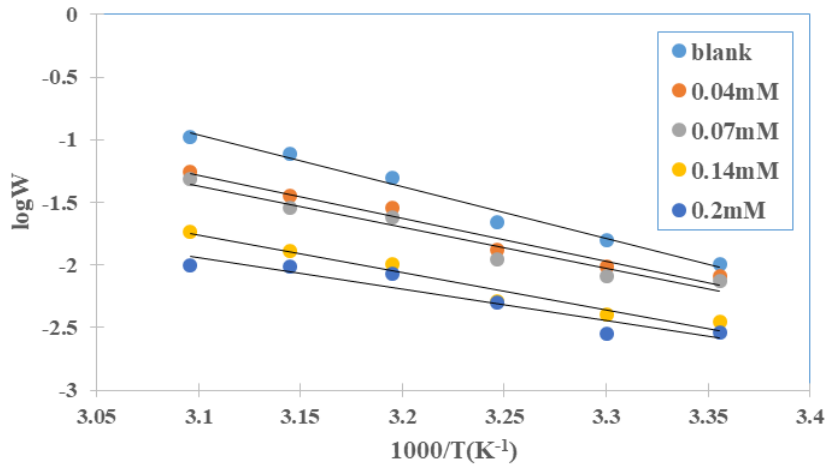

Figure 7. Arrhenius plots for copper corrosion in 1M HNO_3 for DBP different concentrations

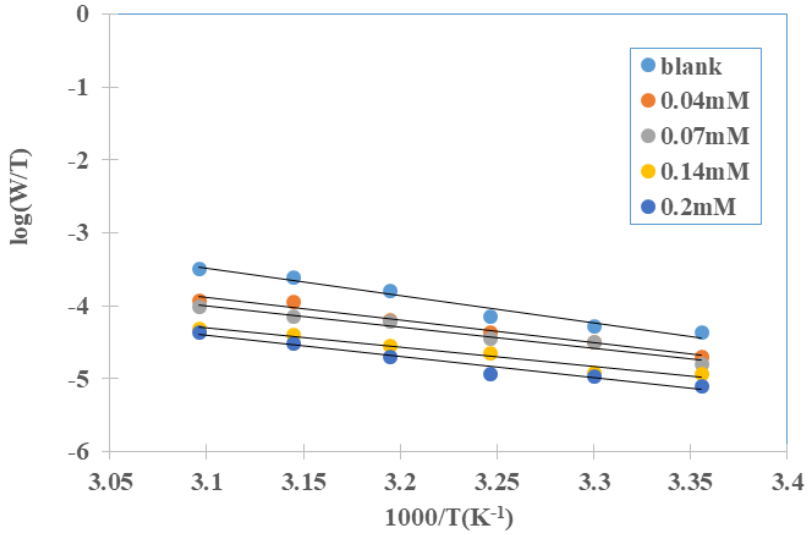

Figure 8. Transition state plots for DBP different concentrations

The apparent activation energy (E_a) was obtained from the slopes of straight lines in Figure 7. The values of activation enthalpy (ΔH_a^*) and activation entropy (ΔS_a^*) were obtained, respectively, from the slopes and intercepts of the straight lines obtained from the plot of log (W/T) versus. 1/T (Figure 8).

All the activation parameter values are recorded in Table 4.

Table 4. Thermodynamic activation parameters of copper dissolution in 1 M HNO_3 in the absence and presence of DBP.

Concentration (mM)	$E_a(kJmol^{-1})$	$\Delta H_a^*(kJmol^{-1})$	$\Delta S_a^*(Jmol^{-1}K^{-1})$
blank	78.9477	70.9825	-44.2073
0.04	57.6013	54.6770	-101.9446
0.07	57.5707	54.5986	-103.8009
0.14	48.9050	44.2717	-142.3371
0.2	39.8968	36.4922	-169.3101

A comparison of the activation energy (E_a) obtained in the presence and absence of an inhibitor provides insight into the nature of adsorption [46]. In our study, the activation energies (E_a) are all positive, and those of the inhibited solutions are higher than those of the blank (uninhibited solution). These observations reveal that the DBP adsorption on the copper surface is dominated by chemisorption. The activation enthalpy (ΔH_a^*) values are positive. In this case, the dissolution process of copper in 1 M nitric acid is endothermic. The values of activation entropy

(ΔS_a^*) are negative, showing that the disorder decreases while passing from the reactant to the activated complex [47].

3.2. Quantum chemistry consideration

3.2.1. Global reactivity

DPB optimized structure is presented in Figure 9. In addition, global reactivity parameter values of DPB obtained from DFT calculations are reported in Table 5.

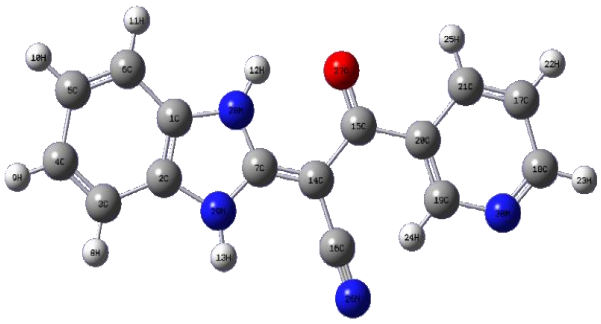

Figure 9. DBP Optimized structure by B3LYP/6-31G (d,p)

Table 5. Quantum Chemical parameters for DPB obtained with DFT at B3LYP/6-31G (d,p) and B3LYP/6-311G (d,p).

Quantum chemical parameters	6-31G (d, p)	6-311G (d, p)
E_{HOMO} (eV)	-7.7558	-5.9909
E_{LUMO} (eV)	-1.8518	-1.8354
Energy gap ΔE (eV)	5.9040	4.1554
Dipole moment μ (D)	6.9687	6.9347
Ionization energy I (eV)	7.7558	5.9909
Electron affinity A (eV)	1.8518	1.8354
Electronegativity χ (eV)	4.8038	3.9132
Hardness η (eV)	2.9520	2.0777
Softness (σ) $(eV)^{-1}$	0.3387	0.4813
Fraction of electron transferred ΔN	0.0298	0.2567
Electrophylicity index ω	3.9090	3.6851
Electroaccepting power ω^+	1.8757	1.9881
Electrodonating power ω^-	6.6795	5.9015
Total energy E_T (Ha)	-866.5479	-871.9604

Experimental results showed that DBP adsorbs on the copper surface. To better explain this adsorption phenomenon, quantum chemical calculations have been solicited. Indeed the chemical reactivity of an organic compound generally depends on the frontier molecular orbitals (FMO), comprising the highest occupied molecular orbital (HOMO), and the lowest unoccupied molecular orbital (LUMO) [48]. In addition, the lower the energy value of the lowest unoccupied molecular orbital (E_{LUMO}), the more likely the molecule can receive electrons. Furthermore, the high energy value of the occupied molecular orbital (E_{HOMO}) indicates that the molecule tends to donate electrons to an appropriate acceptor with low energy vacant orbital [48]. Table 4 shows that DBP has a high value of E_{HOMO} and a low value of E_{LUMO}. Therefore, the electron transfer between copper and DBP is justified by the high inhibition efficiency values obtained experimentally.

The electronic distribution densities of HOMO and LUMO orbitals are represented in Figure 9. The distribution of HOMO and LUMO electronic density appears mainly around the molecule's heteroatoms (N and O). These observations revealed that the donor-acceptor character of the studied molecule could first involve these heteroatoms before extending to the other atoms.

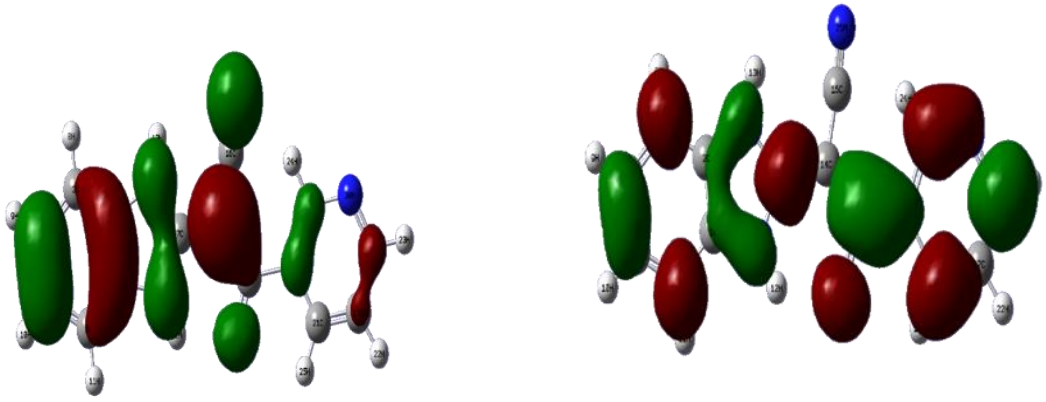

(a) **(b)**

Figure 10. Distribution densities of HOMO **(a)** and LUMO **(b)**

The molecule reactivity depends on its energy gap (ΔE) value. In fact, a more reactive molecule has a low energy gap value while a less reactive molecule has a high energy gap value [49]. Studied molecule has a low energy gap value which is 5.9040eV in base 6-31G(d,p) and 4.1554eV in 6-311G(d, P5, while that of copper is in order of 2.3414eV therefore, it would be easier for HOMO electrons of DBP to migrate to the vacant copper orbital of copper $Cu^{2+}([Ar]3d^9$. These electronic exchanges justify the good inhibition performances of DBP obtained experimentally.

According to literature [50,] account the divergent points of view on dipole moment (μ) dipole, there is no significant relationship between μ values and inhibition.

The low ionization energy (I = 7.7558 eV in 6-31G (d, p) and I = 5.9909 eV in 6-311G (d, p)) value obtained justifies its high inhibition efficiencies obtained experimentally.

In this study, the electronegativity value (χ) of the molecule is lower than that of copper (4.98 eV) in the two-basis set (table 5). Therefore, it results that ΔN > 0. So copper has the best attraction capacity. In this case, there is a possible movement of electrons from the molecule to copper [40]. Similar results have been obtained in previous studies [51].

The studied molecule has the value of low hardness (η) and high softness (σ) in basis sets 6-31G (d, p) and 6-31G (d, p). Therefore, these values show that DBP adsorbs on copper surface [52]. This adsorption is responsible for the best inhibition efficiencies obtained.

Generally, a high electrophilicity index (ω) describes a good electrophile, while a low value indicates a good nucleophile. The values obtained in the basis set show that DBP is a good electrophile, hence its ability to accept electrons from the metal [48]. These observations corroborate with the experimental data.

Electrodonating power (ω^-= 5.9015) value is closer to the value of the ionization potential (I = 5.9909 eV) in the 6-311G (d, p) basis set. This result implies that the molecule can give electrons to the metal. As for the electroaccepting power ($\omega^+ = 1.8757$) value, it is closer to the electron affinity (A = 1.8518) in 6-31G (d, p) basis set. Thus, the tested molecule also has a good ability to accept electrons from the metal. These observations justify the good donor and acceptor capacity of the tested molecule. This could reinforce its ability to protect the metal in the studied solution. Table 5 analysis also informs that hardness (η) is positive, and total energy E_T is negative, which confirms that the inhibitor charge transfer to the metal is energetically favorable. Similar results were obtained in our previous studies [18].

3.2.2. Local reactivity

The Mulliken charges, Fukui indices, and the dual descriptor have been computed to reflect the electrophilic and nucleophilic attack sites. All these quantities are listed in Table 6.

Table 6. Mulliken atomic charges, Fukui functions, and dual descriptor for DBP by B3LYP / 6-31 G (d, p).

Atoms	$q_k(N+1)$	$q_k(N)$	$q_k(N-1)$	f_k^+	f_k^-	$\Delta f_k(\mathbf{r})$
1 C	0.087251	0.236601	-0.016051	-0.14935	0.252652	-0.402002
2 C	0.096382	0.233823	-0.01984	-0.137441	0.253663	-0.391104
3 C	-0.039206	-0.105472	0.133203	0.066266	-0.238675	0.304941
4 C	0.068124	-0.160284	0.038622	0.228408	-0.198906	0.427314

5 C	0.058895	-0.160087	0.022031	0.218982	-0.182118	0.4011
6 C	-0.033724	-0.104986	0.136475	0.071262	-0.241461	0.312723
7 C	-0.131222	0.892071	0.131669	-1.023293	**0.760402**	**-1.783695**
8 H	0.00096	0.178676	-0.007174	-0.177716	0.18585	-0.363566
9 H	-0.00304	0.169311	-0.002544	-0.172351	0.171855	-0.344206
10H	-0.002674	0.169469	-0.001759	-0.172143	0.171228	-0.343371
11H	0.000755	0.182317	-0.007244	-0.181562	0.189561	-0.371123
12H	-0.00433	0.381586	-0.001709	-0.385916	0.383295	-0.769211
13H	-0.004015	0.35067	-0.000508	-0.354685	0.351178	-0.705863
14C	0.561038	-0.32719	-0.074897	0.888228	-0.252293	1.140521
15C	-0.068485	0.628323	0.22429	-0.696808	0.404033	-1.100841
16C	-0.102146	0.288547	0.0085	-0.390693	0.280047	-0.67074
17C	0.01479	-0.234099	-0.0577	0.248889	-0.176399	0.425288
18C	0.022471	0.17187	0.18558	-0.149399	-0.01371	-0.135689
19C	0.034366	0.113893	0.125781	-0.079527	-0.011888	-0.067639
20C	0.02474	-0.158192	0.00969	0.182932	-0.167882	0.350814
21C	-0.011224	-0.042516	0.082188	0.031292	-0.124704	0.155996
22H	-0.000664	0.155513	0.001879	-0.156177	0.153634	-0.309811
23H	-0.001076	0.165895	-0.010204	-0.166971	0.176099	-0.34307
24H	-0.001828	0.209494	-0.006998	-0.211322	0.216492	-0.427814
25H	0.000237	0.191666	-0.004399	-0.191429	0.196065	-0.387494
26N	0.133424	-0.505999	-0.016285	0.639423	-0.489714	1.129137
27O	0.074116	-0.685976	0.154382	0.760092	-0.840358	1.60045
28N	0.125392	-0.818694	0.003303	0.944086	-0.821997	1.766083
29N	0.110222	-0.84903	0.003633	**0.959252**	-0.852663	**1.811915**
30N	-0.009529	-0.5672	-0.033915	0.557671	-0.533285	1.090956

Figure 11 shows the skeleton of 2-(1,3-dihydrobenzimidazol-2-ylidene)-3-oxo-3-(pyridin-3-yl) propanenitrile (DBP) from DFT B3LYP/6-31G (d,p).

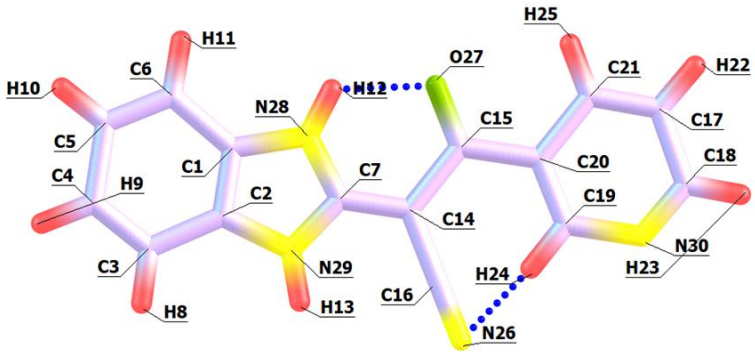

Figure 11. 2-(1,3-dihydrobenzimidazol-2-ylidene)-3-oxo-3-(pyridin-3-yl) propanenitrile (DBP) skeleton.

Local reactivity values parameters recorded in Table 6 indicate that N (29) with the maximum value of f_k^+ and $\Delta f_k(\mathrm{r})$ is the most probable site for nucleophilic attacks. While C (7)), with the total value of f_k^- and the most negative value, $\Delta f_k(\mathrm{r})$ is the most probable site for electrophilic attacks.

3.3. Inhibition Mechanism

DBP inhibition effect can be explained by experimental results, which were justified by theoretical data.

In nitric acid solution, DBP is protonated and will be in equilibrium with its corresponding neutral form according to the following equation:

$$C_{15}H_{10}ON_4 + HNO_3 \rightleftarrows [C_{15}H_{11}ON_4]^+ + NO_3^-$$

The negative charge on copper surface adsorbs protonated form due to sulfate ions NO_3^- presence of nitric acid solution. This adsorption is done on copper by electrostatic bonds: this is physisorption. These bonds are weak. This type of bond is sensitive to temperature and does not allow to fight effectively against corrosion at high temperatures.

DBP adsorbs onto the copper surface through donor-acceptor interactions between the free electron pairs of heteroatoms and the π-electron system of aromatic rings. These electron transfers create a copper-inhibitor complex on the copper surface, showing chemisorption existence. These electron transfers are justified by the values of quantum chemical parameters such as fraction electrons transferred (ΔN), E_{HOMO}, E_{LUMO}, and energy gap (ΔE) that the studied molecule displays. The complex formed is resistant to high temperatures, which justifies the values of IE at high temperatures showing the predominance of chemisorption. The mechanism of inhibition is illustrated in the figure below.

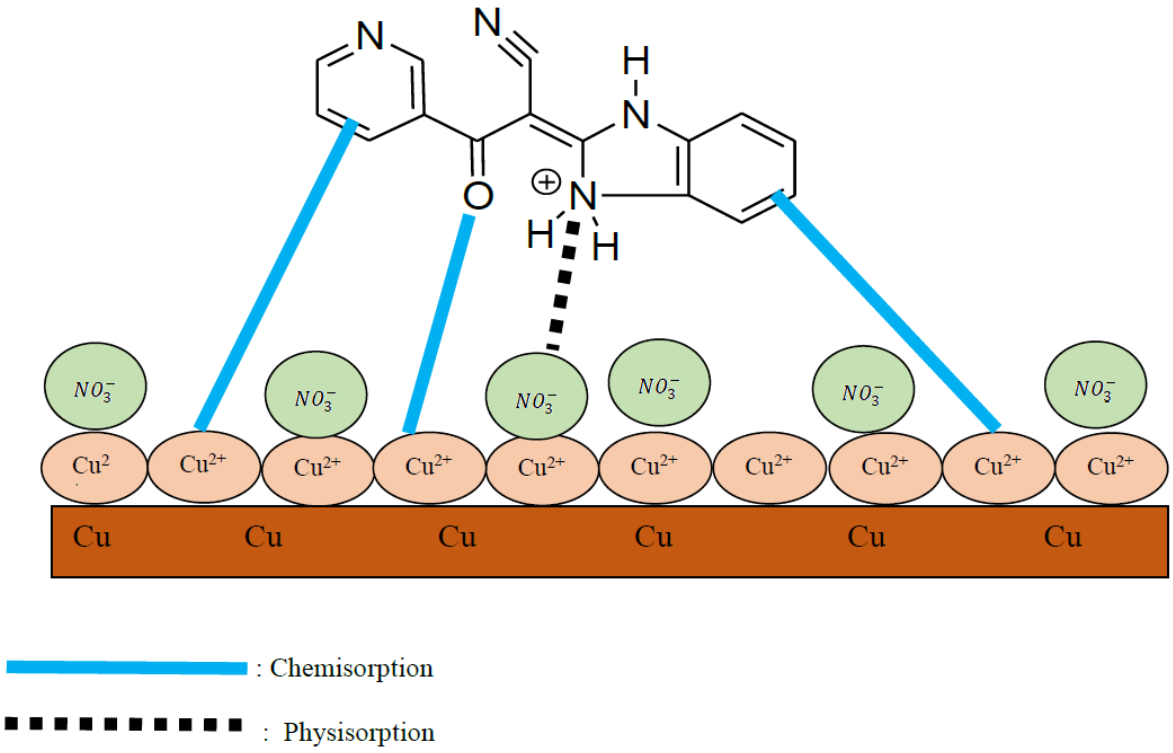

Figure 12. Schematic representation of copper corrosion inhibition mechanism by DBP

3.4. Quantitative Structure-Property Relationship (QSPR) assessment

QSPR model consists of finding a set of quantum chemical parameters that will correlate the experimental data (experimental inhibition efficiency) and theoretical data (calculated inhibition efficiency). So, the different coefficient values calculated with EXCEL software for the different sets of parameters are recorded in Table 8. The values of inhibition efficiencies at 298 K (Table 7) have been used for this part.

Table 7. Inhibition efficiencies of DBP at 298 K for different concentrations.

Concentration(mM)	IE (%)
0.04	25.0067
0.07	38.1305
0.14	62.5033
0.2	68.7528

Table 8. Calculated constants of the different sets of parameters.

Set of parameters	A	B	D	E
$(\Delta E, I, A)$	3.436X10^{12}	-1.3744X10^{12}	-166.666667	-9.6207X10^{12}
$(\eta, \sigma, \Delta N)$	0.11712299	-4.08653846	-0.72115385	0.50448718
$(\omega, \mu, \Delta E)$	-8	-9.5	-119.06	667.45
$(E_{HOMO}, E_{LUMO}, \chi)$	-70.8333333	33.3333333	24.780303	-606.228788

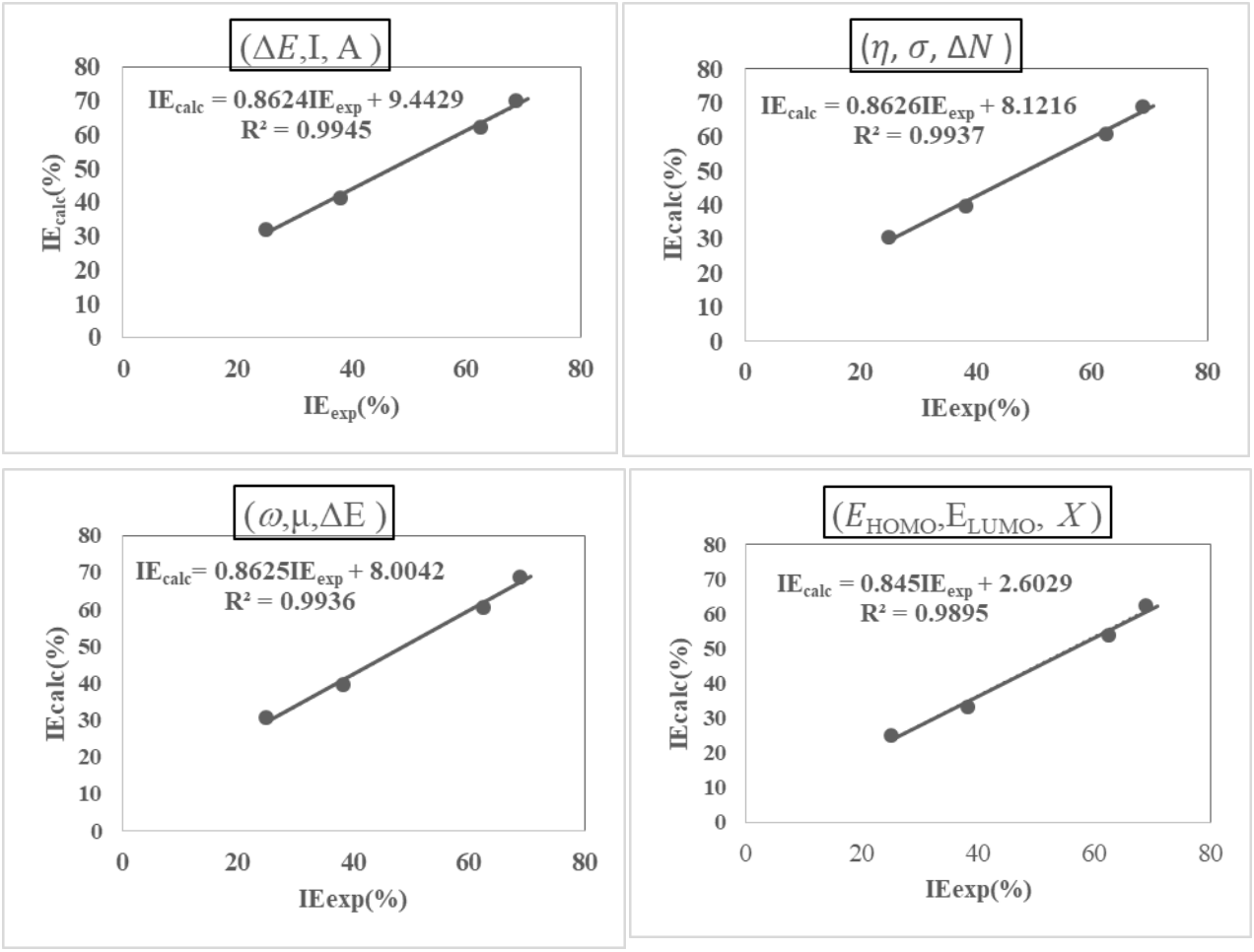

Figure 12. Calculated versus experimental inhibition efficiencies for a different set of parameters

The statistical parameters were determined to correctly identify the best parameters that could correlate with the experimental and theoretical inhibition efficiencies. These parameters are expressed as follows [38]:

The sum of square errors (SSE):

$$SSE = \sum_{i=1}^{N}\left(IE_{exp} - IE_{calc}\right)^2 \quad (31)$$

The root means square error (RMSE):

$$RMSE = \sqrt{\frac{\sum_{i=1}^{N}\left(IE_{exp} - IE_{calc}\right)^2}{N}} \quad (32)$$

The Mean Percent Deviation (MPD):

$$MPD = \frac{1}{N}\sum_{i=1}^{N}\left|\frac{\left(IE_{\exp} - IE_{calc}\right)}{IE_{\exp}}\right| \quad (33)$$

Table 9. Determination coefficients statistical parameters of different sets.

Set of parameters	R^2	SSE	RMSE	MPD
$(\Delta E, I, A)$	0.9945	59.6031	3.8601	0.0961
$(\eta, \sigma, \Delta N)$	0.9937	38.1727	3.0892	0.07548
$(\omega, \mu, \Delta E)$	**0.9936**	**36.9600**	**3.0397**	**0.0736**
$(E_{HOMO}, E_{LUMO}, \chi)$	0.9895	137.8725	5.8709	0.0888

Examination of Table 9 about statistical parameters and determination coefficients shows that $(\omega, \mu, \Delta E)$ can be considered as the best set of parameters to correlate theoretical and experimental results. Indeed, these parameters' statistical coefficients (SSE, RMSE, MPD) have low values. In addition, the value of Mean Percent Deviation (MPD = 0.0736) confirms the consistency between experimental and theoretical results determined using QSPR model. This excellent correlation between the observed values obtained and the calculated values ($R^2 > 0.99$) is due to DBP good solubility in 1 M nitric acid solution.

4. Conclusion

The mass loss technique showed that DBP is an effective inhibitor of copper corrosion in 1 M HNO_3 solution. The copper corrosion rate increases with temperature and decreases with increasing DBP concentration. DBP inhibition efficiency depends on temperature and concentration. According to Langmuir isotherm, the isotherms adsorption study showed that the molecule adsorbs on the copper surface. Adejo - Ekwenchi isotherm showed that this adsorption is dominated by chemisorption. The thermodynamic parameters adsorption and activation revealed that the adsorption process is spontaneous and endothermic, and the adsorbed layer is stable with the predominance of chemisorption. The quantum chemical parameters from DFT calculations explained the interactions between copper and DBP. These interactions are essentially based on electronic exchanges between the two entities. Then the local reactivity parameters such as Fukui functions $(f(r))$ and dual descriptor $(\Delta f_k(\mathrm{r}))$ indicated the probable sites of electrophilic and nucleophilic attacks within the molecule. Finally, the quantitative structure-property relationship (QSPR) model showed that the parameter set $(\omega, \mu, \Delta E)$ permits showing a good correlation between theoretical parameters and experimental results.QSPR is also sufficient to predict the efficiencies of analogous molecules using the theoretical approach. There is a good consistency between the experimental and theoretical results.

Acknowledgments

The authors gratefully acknowledged the support of the Laboratory of Environmental Sciences and Technologies at Jean Lorougnon Guede University of Daloa (Côte d'Ivoire) and the Laboratory of Constitution and Reaction of Matter of Felix Houphouët Boigny University of Abidjan (Côte d'Ivoire).

References

1- L. Zhou, S. Zhang, B. Tan, L. Feng, B. Xiang, F. Chen, W. Li, B. Xiong, T. Song, Phenothiazine drugs as novel and eco-friendly corrosion inhibitors for copper in sulfuric acid solution, Journal of the Taiwan Institute of Chemical Engineers, **2020**, 113, 253–263.
2- J. Zhang, L. Zhang, G. Tao, A novel and high-efficiency inhibitor of 5-(4-methoxyphenyl)-3h-1,2-dithiole-3-thione for copper corrosion inhibition in sulfuric acid at different temperatures, Journal of Molecular Liquids, **2018**, 272, 369-379.
3- A. Hedin, J. Johansson, F. King, Comment on Corrosion-induced microstructure degradation of copper in sulfide-containing simulated anoxic groundwater studied by synchrotron high-energy X-ray diffraction and ab-initio density functional theory calculation, Corrosion Science, **2022**, 199, 110182.
4- A. Jmiai, A. Tara, S. El Issami, M. Hilali, O. Jbara, L. Bazzi, A new trend in corrosion protection of copper in acidic medium by using Jujube shell extract as an effective green and environmentally safe corrosion inhibitor: Experimental, quantum chemistry approach and Monte Carlo simulation study, Journal of Molecular Liquids, **2021**, 322, 114509, 1-36.
5- S. Echihi, N. Benzbiri, M. E. Belghiti, M. ElFal, M. Boudali, E. M. Essassi, A. Guenbour, A. Bellaouchou, M. Tabyaoui, M. Azzib, Corrosion inhibition of copper by pyrazole pyrimidine derivative in synthetic seawater: Experimental and theoretical studies, Materialstoday Proceedings, **2021**, 37(2), 3958-3966.
6- R. Laggoun, M. Ferhat, B. Saidat, A. Benghia, A. Chaabani, Effect of p-toluenesulfonyl hydrazide on copper corrosion in hydrochloric acid solution. Corrosion Science, **2020**, 165, 108363.
7- L. Guo, B. Tan, X. Zuo, W. Li, S. Leng, X. Zheng, Eco-friendly food spice 2-Furfurylthio-3-methylpyrazine as an excellent inhibitor for copper corrosion in sulfuric acid medium, Journal of Molecular Liquids, **2020**, 317, 113915.
8- L. Zhou, S. Zhang,B. Tan,Li Feng, B. Xiang, F. Chen, Weining Li, B. Xiong, T. Song, Phenothiazine drugs as novel and eco-friendly corrosion inhibitors for copper in sulfuric acid solution, Journal of the Taiwan Institute of Chemical Engineers, **2020**, 113, 253-263.
9- A. K. Singh, S. Mohapatra, B. Pani, Corrosion Inhibition Effect of Aloe Vera gel: Gravimetric and Electrochemical Study, Journal of Industrial and Engineering Chemistry, **2016**, 25, 288-297.
10- M. A. Deyab, Egyptian Licorice Extract as a Green Corrosion Inhibitor for Copper in Hydrochloric Acid Solution, Journal of Industrial and Engineering Chemistry, **2015**, 25, 384-389.
11- B. S. Mahdi, H. S. S. Aljibori, M. K. Abbass, W. K. Al-Azzawi, A. H. Kadhum, M. M. Hanoon, W. N. R. W. Isahak, A. A. Al-Amiery, H. Sh. Majdi, Gravimetric analysis and quantum chemical assessment of

4-aminoantipyrine derivatives as corrosion inhibitors, International Journal of Corrosion and Scale Inhibition, **2022**, 11(3), 1191–1213

12- K. El Mouaden, D. S. Chauhan, M. A. Quraishi, L. Bazzi, M. Hilali, Cinnamaldehyde-modified chitosan as a bio-derived corrosion inhibitor for acid pickling of copper: Microwave synthesis, experimental and computational study, International Journal of Biological Macromolecules, **2020**, 164, 3709–3717.

13- S. Smagill, C. Shields, C. L. Sears, M. Choti, W. G. Merz, Résistance croisée aux dérivés triazolés chez Candida sp. : Observation, fréquence dans les isolats sanguins et implications pour les traitements antifongiques Journal de mycologie médicale, **2007**, 17 (1), S1-S10.

14- V. Djohan, K. E. Angora, A. H. Vanga-Bosson, A. Konaté, F. K. Kassi, W. Yavo, P. C. Kiki Barro, In vitro susceptibility of vaginal Candida albicans to antifungal drugs in Abidjan (Ivory Coast), Journal de Mycologie Médicale, **2012**, 22 (2), 129-133.

15- H.J. Al-Fahemi, M.Abdallah, Elshafie A.M.Gad, B.A.A.L.Jahdaly, Experimental and theoretical approach studies for melatonin drug as safely corrosion inhibitors for carbon steel using DFT, Journal of Molecular Liquids,2016,222, 1157-1163

16- M. Abdallah, A. Al Bahira, H. M. Altass, A. Fawzy, N. El Guesmi, A. S. Al-Gorair, F. B.Warad, A. Zarrouk, Anticorrosion and adsorption performance of expired antibacterial drugs on Sabic iron corrosion in HCl solution: Chemical, electrochemical and theoretical approach, Journal of Molecular Liquids, **2021**, 330, 115702, 1-15.

17- H. A. Almashhadani, M. K. Alshujery, M. Khalil, M. M. Kadhemd, A. A. Khadom Corrosion inhibition behavior of expired diclofenac Sodium drug for Al 6061 alloy in aqueous media: Electrochemical, morphological, and theoretical investigations, Journal of Molecular Liquids, **2021**, 117656

18- M. A. Tigori, A. Kouyaté, V. Kouakou, P. M. Niamien, A. Trokourey, Computational approach for predicting the adsorption properties and inhibition of some antiretroviral drugs on copper corrosion in HNO_3, European Journal of Chemistry, **2020**, 11(3), 235-244.

19- M. A. Tigori, A. Kouyaté, V. Kouakou, P. M. Niamien, A. Trokourey, Inhibition Performance of Some Sulfonylurea on Copper Corrosion in Nitric Acid Solution, Evaluated Theoretically by DFT Calculations, Open Journal of Physical Chemistry, **2020**,10(3),139-157.

20- F. J. Rodríguez-Gómez, M. P. Valdelamar, A. E. Vazquez, P. D. Valle Perez, R. Mata, A. Miralrio, M. Castro, Mycophenolic acid as a corrosion inhibitor of carbon steel in 3% wt. NaCl solution. An experimental and theoretical study, Journal of Molecular Structure, **2019**, 1183, 168-181.

21- L. Guo, S. Zhu, S. Zhang, Q. He, W. Li, Theoretical studies of three triazole derivatives as corrosion inhibitors for mild steel in acidic medium, Corrosion Science, **2014**, 87, 366-375.

22- J. A. Van Allan, B. D. Deagon, Organic Syntheses Collect, John Wiley & Sons, New York, NY, USA, 4, **1963**.

23- N. Perin, L. Uzelac, I. Piantanida, G. Karminski-Zamola, M. Kralj, M. Hranjec, Novel biologically active nitro and amino substituted benzimidazo[1,2-a]quinolines Bioorganic & Medicinal Chemistry, **2011**,19 (21), 6329-6339

24- M. J. Frisch, G. W. Trucks, H. B. Schlegel, G. E. Scuseria, M. A. Robb, J. R. Cheeseman, G. Scalmani, V.Barone, B. Mennucci, G. A. Petersson, H. Nakatsuji, M. Caricato, X. Li, H. P. Hratchian, A. F. Izmaylov, J.Bloino, G. Zheng, J. L. Sonnenberg, M. Hada, M. Ehara, K. Toyota, R. Fukuda, J. Hasegawa, M. Ishida, T.Nakajima, Y. Honda, O. Kitao, H. Nakai, T. Vreven, J. A. Montgomery, Jr., J. E. Peralta, F. Ogliaro, M.Bearpark, J. J. Heyd, E. Brothers, K. N. Kudin, V. N. Staroverov, R. Kobayashi, J. Normand, K. Raghavachari,A. Rendell, J. C. Burant, S. S. Iyengar, J. Tomasi, M. Cossi, N. Rega, J. M. Millam, M. Klene, J. E. Knox, J. B.Cross, V. Bakken, C. Adamo, J. Jaramillo, R. Gomperts, R. E. Stratmann, O. Yazyev, A. J. Austin, R. Cammi,C. Pomelli, J. W. Ochterski, R. L. Martin, K. Morokuma, V. G. Zakrzewski, G. A. Voth, P. Salvador, J. J.Dannenberg, S. Dapprich, A. D. Daniels, Ö. Farkas, J. B. Foresman, J. V. Ortiz, J. Cioslowski and A. D. J. Fox,Gaussian, Inc., Wallingford, 09.**2009**

25- A. D. Becke, Density-functional thermochemistry. I. The effect of the exchange-only gradient correction, The Journal of Chemical Physics, **1992**, 96, 2155-2160.

26- C. Lee, W. Yang, R. G. Parr, Development of the Colle-Salvetti correlation-energy formula into a functional of the electron density, Physical Review B., **1988**, 37, 785-789.

27- H. Allal, Y. Belhocine, E. Zouaoui, Computational study of some thiophene derivatives as aluminium corrosion inhibitors, Journal of Molecular Liquids, **2018**, 265, 668–678.

28- T. Koopmans, Uber die Zuordnung von Wellenfunktionen und Eigenwerten zu den Einzelnen Elektronen Eines Atoms, Physica A: Statistical Mechanics and its Applications, **1934**, 1(1–6), 104–113.

29- H. Al-Fahemi, M. Abdallah, E. A. M. Gad, B. A. A. L. Jahdaly, Experimental and theoretical approach studies for melatonin drug as safely corrosion inhibitors for carbon steel using DFT, Journal of Molecular Liquids, **2016**, 222, 1157–1163.

30- R. G. Pearson, "Hard and soft acids and bases-the evolution of a chemical concept," Coordination Chemistry Reviews, **1990**, 100, 403–425.

31- H. B. Michaelson, The work function of the elements and its periodicity, Journal of Applied Physics, **1977**, 48, 4729-4733.

32- M. J. S.Dewar, E. G.Zoebisch, E. F. Healy, J. P. Stewart, Development and use of quantum mechanical molecular models, 76, AM1: a new general-purpose quantum mechanical molecular model, Journal of the American Chemical Society, **1985**, 107(13), 3902-3909.

33- R. G. Parr, L. V. Szentpaly, S. Liu, Electrophilicity index,' Journal of the American Chemical Society, **1999**, 121(9), 1922–1924.

34- J. L. Gazquez, A. Cedillo, A. Vela, Electrodonating and electroaccepting powers, The Journal of Physical Chemistry, **2007**, 111, 1966-1970.

35- A. Berrissoul, A. Ouarhach, F. Benhiba, A. Romane, A. Zarrouk, A. Guenbour, B. Dikici, A. Dafali, Evaluation of Lavandula mairei extract as green inhibitor for mild steel corrosion in 1 M HCl solution. Experimental and theoretical approach, Journal of Molecular Liquids, **2020**, 313, 113493.

36- C. Morell, A. Grand, A. Toro-Labbé, New Dual Descriptor for Chemical Reactivity, Journal of Physical Chemistry. A, **2005**, 109, 205-212.

37- J. I. Martínez-Araya, Why Is the Dual Descriptor a More Accurate Local Reactivity Descriptor than Fukui Functions, Journal of Mathematical Chemistry, **2015**, 5, 451-465.

38- N. O. Obi-Egbedi, I. B. Obot, M. I. El-Khaiary, S. A. Umoren, E. E. Ebenso, Computational Simulation and Statistical Analysis on the Relationship Between Corrosion Inhibition Efficiency and Molecular Structure of Some Phenanthroline Derivatives on Mild Steel Surface, International Journal of electrochemical science, **2011**, 6, 5649 – 5675.

39- I. Lukovits, E. F. Kalman, Corrosion Inhibitors—Correlation between Electronic Structure and Efficiency, Corrosion, **2001**, 57(1), 3-8.

40- Z. Žaklina, B. TasićMarija, P. Mihajlović, M. B. Radovanović, A. T. Simonović, M. M. Antonijević, Experimental and theoretical studies of paracetamol as a copper corrosion inhibitor, Journal of Molecular Liquids, **2021**, 327, 114817, 1-9.

41- A. Fawzy, I. A. Zaafarany, H. M. Ali, M. Abdallah, New synthesized amino acids-based surfactants as efficient inhibitors for corrosion of mild steel in hydrochloric acid medium: kinetics and thermodynamic approach, International Journal of electrochemical science, **2018**, 13, 4575–4600.

42- N. Benzbiria, S. Echihi, M. E. Belghiti, A. Thoume, A. Elmakssoudi, A. Zarrouk, M. Zertoubi, M. Azzi Novel synthesized benzodiazepine as efficient corrosion inhibitor for copper in 3.5% NaCl solution, Materials Today: Proceedings, **2021**, 37(3), 3932-3939.

43- H. Huang, X. Guo, The relationship between the inhibition performances of three benzo derivatives and their structures on the corrosion of copper in 3.5 wt.% NaCl solution, Colloids and Surfaces A: Physicochemical and Engineering Aspects, **2020**, 598, 124809.

44- R. Farahati, H. Behzadi, S. M. Mousavi-Khoshdel, A. Ghaffarinejad, Evaluation of corrosion inhibition of 4-(pyridin-3-yl) thiazol-2-amine for copper in HCl by experimental and theoretical studies, Journal of Molecular Structure, **2020**, 1205, 127658.

45- S. O. Adejo, M. M. Ekwenchi, Resolution of adsorption characterization ambiguity through the Adejo-Ekwenchi adsorption isotherm: a case study of leaf extract of Hyptis suaveolen point as green corrosion inhibitor of corrosion of mild steel in 2 M HCl, Journal of Emerging Trends in Engineering and Applied Sciences, **2014**, 5, 201- 205.

46- M. Abdallah, A. Fawzy, A. Al Bahir, The effect of expired acyclovir and omeprazole drugs on the inhibition of Sabic Iron corrosion in HCl solution, International Journal of electrochemical science15, **2020**, 15, 4739–4753.

47- Y. Qiang, S. Zhangao, S. Yan, X. Zou, S. Chen, Three indazole derivatives as corrosion inhibitors of copper in a neutral chloride solution, Corrosion Science, **2017**, 126, 295-304.

48- M. Khattabi, F. Benhiba, S. Tabti, A. Djedouani, A. El Assyry, R. Touzani, I. Warad, H. Oudda, A. Zarrouk, Performance and computational studies of two soluble pyran derivatives as corrosion inhibitors for mild steel in HCl, Journal of Molecular Structure, **2019**, 1196, 231-244

49- A Singh, K. R Ansari, A. Kumar, W. Liu, C. Songsong, Y. Liu, Electrochemical, surface and quantum chemical studies of novel imidazole derivatives as corrosion inhibitors for J55 steel in a sweet corrosive environment, Journal of Alloys and Compounds, **2017**, 712, 121-133.

50- R. Padash, M. Rahimi-Nasrabadi, A. Shokuhi Rad, A. Sobhani-Nasab, T. Jesionowski, H. Ehrlich, A theoretical study of two novel Schiff bases as inhibitors of carbon steel corrosion in acidic medium, Applied Physics A, **2019**,125,1-11

51- Z. Z. Tasić, M. B. Petrović Mihajlović, A. T. Simonović, M. B. Radovanović, M. M. Antonijević, Ibuprofen as a corrosion inhibitor for copper in synthetic acid rain solution, Scienfic Reports, **2019**, 9(1), 14710.

52- B. Hamrahi, A. Khanlarkhani, S. Morteza Madani, A. Fattah-alhosseini, S. O. Gashti, Evaluation of Henna Extract Performance on Corrosion Inhibition of API 5L Steel in H_2S-Containing Medium and DFT Quantum Computing of Its Constituents, Metals and Materials International, **2021**, 27, 4463–4476.